

Mechanisms Involved in Maturation of Clay Seals in Boreholes for Storing Spent Reactor Fuel

Roland Pusch¹, Jörn Kasbohm², Thao Hoang-Minh³ and Lan Nguyen-Thanh⁴

Abstract

Smectite clay, especially montmorillonite, is proposed for isolating canisters containing highly radioactive waste (HLW) like spent reactor fuel placed in deep boreholes. It is used for minimizing groundwater flow around and along waste packages (“Buffer Clay”) and for providing them with ductile embedment for eliminating risk of canister damage caused by displacements in the host rock. The clay has the form of heavily compacted blocks of granules that swell in conjunction with water uptake until their full hydration potential has been utilized. The dense clay blocks are fitted in perforated supercontainers that are submerged in smectite mud. The long-term chemical stability of the clay is sufficient for providing the required waste-isolating capacity, which is primarily supplied by the heaviness of stagnant, very salt groundwater at depth.

Keywords: Smectite clay, montmorillonite, isolating canisters, highly radioactive waste (HLW), supercontainers, dry density, settlement, creep settlement, microstructure of smectite clay.

¹ Luleå University of Technology, Sweden

² Greifswald University, Germany

³ Greifswald University, Germany

⁴ Technical University of Darmstadt, Germany.

1. Introduction

We will consider here the evolution of "Buffer" clay components in repositories for spent nuclear fuel consisting of deep holes with 0.6-0.8 m diameter bored in crystalline rock (Figure 1). The paper describes major physico-chemical mechanisms involved in the maturation of clay seals, i.e. expansion/consolidation, shear strain, and migration of water and radionuclides. Table 1 exemplifies clay materials that are commercially available and provide effective isolation of HLW. It summarizes typical properties of three types of smectitic clay referred to throughout the paper. The values stem from tests of such clay materials saturated with low- to high-calcium chloride concentrations. The swelling pressure is a practical measure of the expandability of the clay [1]. Special conditions prevail in deeply located repositories represented here by a concept named VDH (Very Deep Holes), which is one of several possible versions [2].

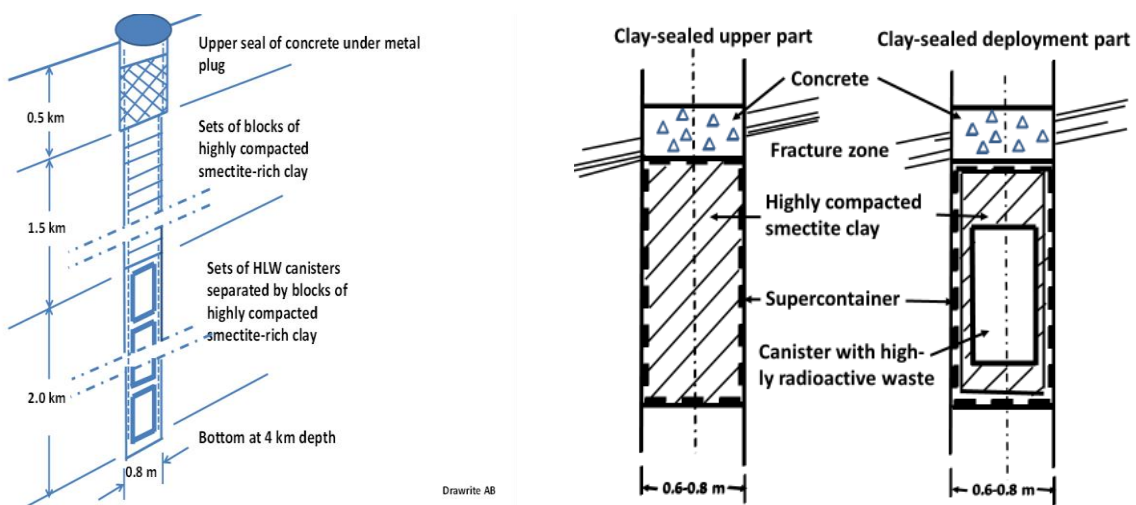


Figure 1: Deep hole concept "VDH". In the upper parts highly compacted clay seals the holes. In the lower, "deployment" zone (2-4 km), sets of "supercontainers" with high-level radioactive waste is embedded in dense clay, and separated by very dense clay blocks. The supercontainers of copper or Navy Bronze, steel or titanium will be submerged in soft clay mud [3].

Table 1: Typical geotechnical properties of clay seal materials saturated with distilled water and 3.5% calcium chloride solution, respectively. K is hydraulic conductivity and p_s swelling pressure (index d= distilled water and index s= salt water).

Smectite clay	Dry density [kg/m ³]	Hydraulic conductivity K_d/K_s [m/s]	Swelling pressure p_{sd}/ p_{ss} [kPa]
Montmorillonite	1,350	5E-12/4E-12	1,020
Saponite	1,020	4E-12	1,250
Mixed-layer illite/montmorillonite	1,530	E-12	1,200

One notices that the three clay types have approximately the same hydraulic conductivity and expandability but for quite different dry densities. For the case in focus here, i.e. deep boreholes, the clay in the upper part of the holes will not be exposed to higher temperature than 60-70°C, whereas in the lower, waste-bearing part, it will be heated up to 150°C for up to a few hundred years. The differences in temperature and salinity affect the properties of the clay as described in the paper.

2. Microstructural constitution

2.1 Basics

Figure 2 depicts schematically the crystal structure of the expandable part of the dominant clay minerals of the three reference clays montmorillonite, saponite and mixed-layer clay.

Figure 3 shows transmission electron micrographs of microstructural organisation of the respective clay mineral type. Figure 3 shows electron micrographs of the reference clays with similar dry densities. The three reference clay minerals, montmorillonite, saponite and smectite/illite mixed-layer clay are characterized by domains of stacked lamellae with water molecule hydrates in the interlamellar space. Montmorillonite is the most expandable type and is the only expandable species that can have up to 3 interlamellar hydrates at saturation with Na and Mg [4].

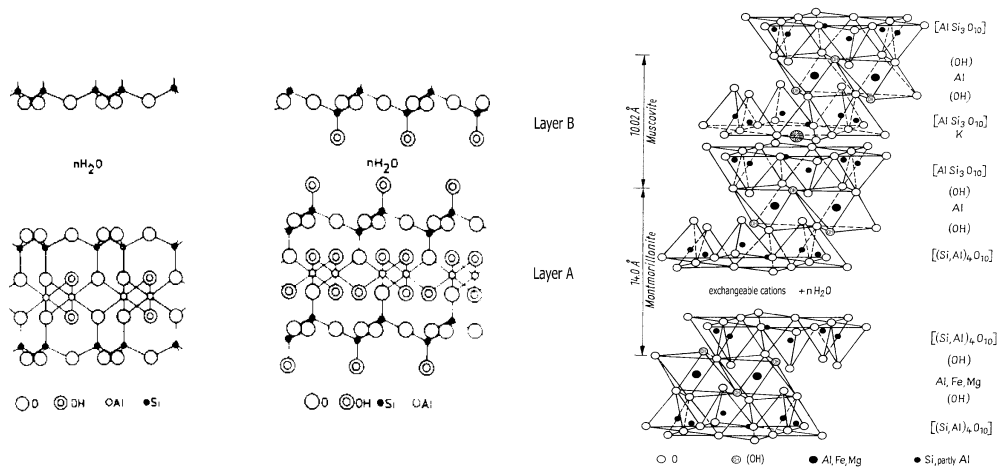


Figure 2: Left and central: Two possible montmorillonite crystal structures with Al in the octahedral sheet, the left one being valid also for saponite except that Mg is in the octahedral sheet. Right: Illite/muscovite mixed layer clay mineral (Friedland clay).

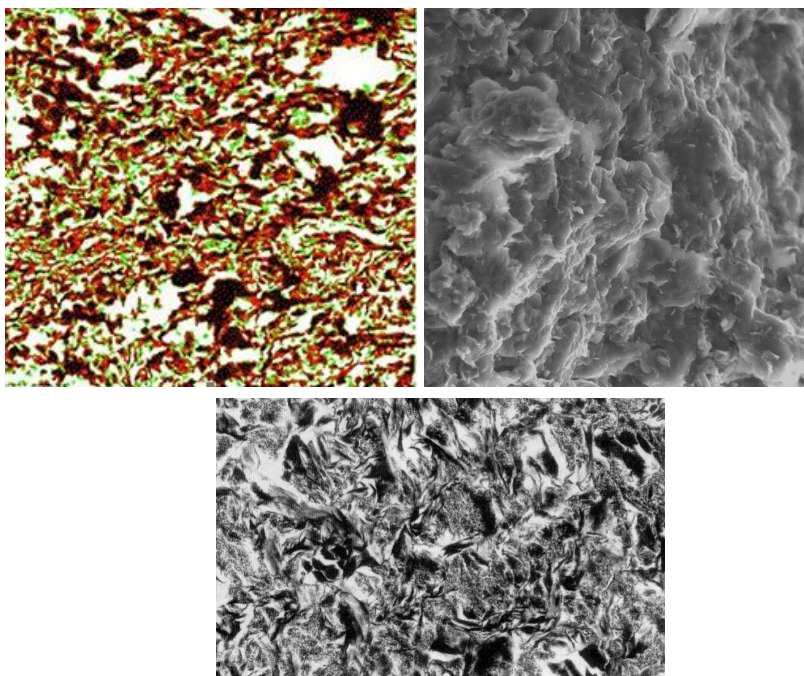


Figure 3: Electron micrographs of reference clays with a dry density of about 1300-1400 kg/m³. Upper left: Transmission micrograph of Montmorillonite (Black=densest part of clay matrix, Red= medium-dense matrix, Green=softest matrix, White=open void). Upper right: Scanning micrograph of Saponite. Lower: Transmission micrograph of Illite/smectite mixed layer clay (Friedland clay). Length of the bar is 1 μm.

2.2 Correlation of microstructural and bulk physical

2.2.1 Generalized microstructural model of smectitic clay

We focus here on clay-isolated highly radioactive waste in the form of spent nuclear fuel contained in metal canisters lined with dense clay, in turn contained in cylindrical supercontainers placed in deep holes bored in crystalline rock. The clay linings and blocks make up the "buffer" that serves to isolate them from rock movements and groundwater flow. The clay must fulfill strict criteria in respect to hydraulic performance, gas and heat conductivity as well as to rheological behaviour. It must also have robust performance characteristics and longevity, which is fulfilled by very dense montmorillonite or saponite (Mg-smectite).

The requirement that the extremely low hydraulic conductivity of the smectite buffer shall be maintained for periods of hundreds of thousands of years makes the longevity particularly important [5]. There is also need to retard diffusive transport of errant radionuclides such that they would be harmless when emerging on land surface environment. The necessary retardation time period ranges between 10,000 and 1,000,000 years. In this context one has to recognize that the temperature of the canisters with HLW can reach 150°C for a few centuries, which very significantly speeds up both flow and diffusion of contaminated porewater.

2.2.2 Constitution and motion of porewater and electrolytes

Comprehensive investigations of the physical state and properties of porewater in clay have been made by various scientists. Particular effort has been put in interpreting the behaviour of water at and around the freezing point which has led to models like the one shown in Figure 4. It ascribes reduced mobility of the water closest to mineral surfaces ("Water A") with 0.003- 0.004Pas⁻¹ viscosity extending to about 1-2nm distance from montmorillonite base-planes, and 0.0015Pas viscosity for water within 2-4nm distance from base-planes. In Water B ice crystals and lenses begin to form if the temperature drops sufficiently much. Energy conditions successively bring ordinary free water ("Water C") with <0.001 Pas⁻¹ viscosity, to become interchanged with "Water B" [6].

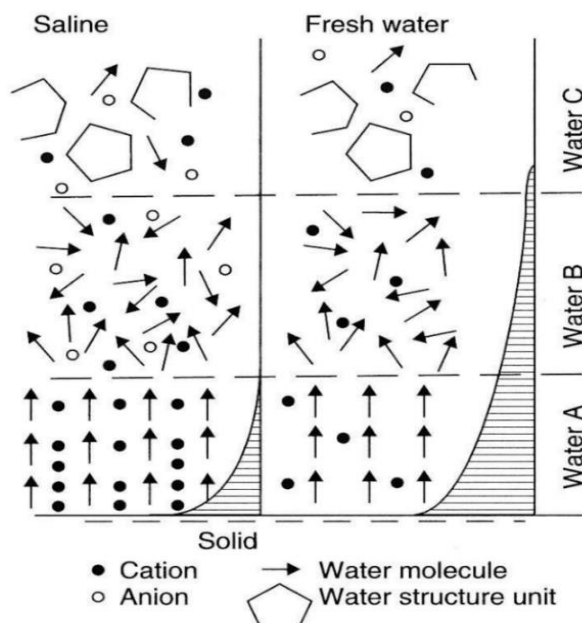


Figure 4: Differences in water structure adjacent to the mineral surfaces in montmorillonite in salt and fresh water, respectively. Water A is most strongly mineral-bound and has higher viscosity, Water B is least viscous and controls formation of ice lenses at freezing, and Water C is free from mineral influence (After Drost-Hansen).

2.2.3 Impact of clay microstructure on the motion of water and electrolytes

Colloid chemistry has helped to understand and quantify motion of electrolytes in smectite clay like montmorillonite. Basic phenomena are for example the exclusion of anions from the interlamellar space in such clays because of the negative charge of the smectite crystal lattices (“Donnan exclusion”), and partial exclusion of any ions from very narrow channels in the clay microstructure (cf. Figure 5).

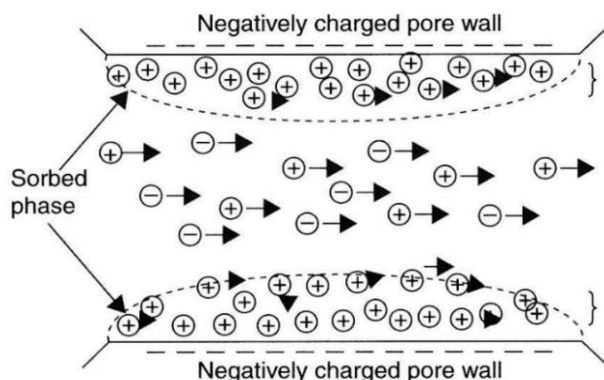


Figure 5: Distribution of cation and anions in percolated voids in montmorillonite clay. Consolidation under external effective pressure closes the central space which will ultimately contain only cations (After Neretnieks).

The cat- and anions are not uniformly distributed in the clay-water matrix as indicated in Figures 5 and 6. Thus, the interlamellar porewater, which is free from anions, cannot be distinguished from the free porewater C in Figure 4, and ordinary chemical analysis only gives the average composition. Expulsion of porewater under successively increased pressure shows a change in composition since low pressures expel water contained in large voids while high pressures cause water from small voids and channels and from the interlamellar space to be released [7]. The practical meaning of this is that the dry density of smectitic clay seals should be as high as possible for minimizing diffusive migration of radionuclides in ionic form.

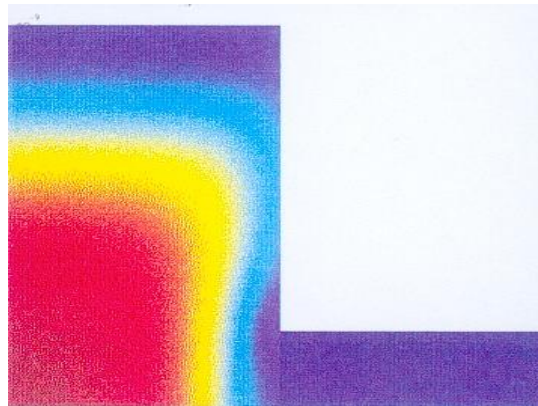


Figure 6: Relative monovalent anion concentration (%) in a representative volume (REV) for equilibrating 0.1 M monovalent electrolyte in MX-80 clay with a density at water saturation of 2130kg/m³. The picture shows that anions (red and yellow) are confined in the center of the widest channels (50 μ m) and that cations (blue) are close to the mineral surfaces and totally dominant in the channels (After Lehikoinen, cf. [7]).

Another implication of the diagram in Figure 5 is that the large majority of the channels in dense hydrated buffer clay contains viscous porewater saturated with cations and that any forced percolation will set up electric potentials that counteract and retard water migration [8]. The compression of dual porosity soil has been treated theoretically by Murad et al [9], who considered porous systems with dual porosity, in principle consisting of a porous particle matrix composed of permeable particle aggregates with micropores. Their approach is basically that of fundamental soil mechanics, making use of Terzaghi's (1942 and Biot's (1955) theories of primary and secondary consolidation [10,11]. The first is related to macroscopic processes, primarily stress-generated size reduction of macropores that provide most of the permeability, and the second depending on the effect of stress/strain on microscale. Murad et al considered the primary consolidation to be related to compression of the coarse-grained structure, the rate of which is controlled by dissipation of the load-generated porewater pressure, and secondary consolidation the rate of which is dictated by creep of the particle skeleton. This view is also held by the present authors who consider the creep strain to be partly related to shear-induced strain where significant microstructural distortion takes place as exemplified by Figure 7, and creep by accumulation of atomic motions on the microscale in all parts of the clay element.

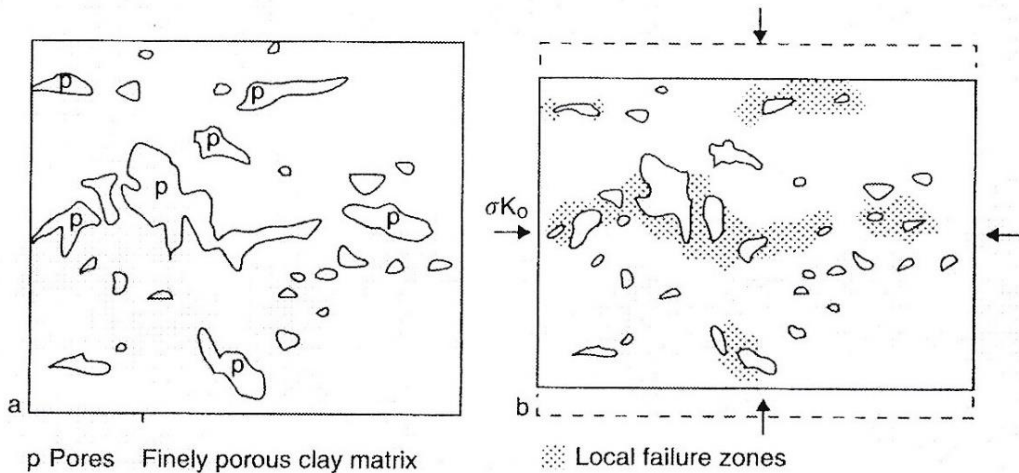


Figure 7: Microstructural changes by compression. The largest voids and channels are compressed first in conjunction with shear-induced breakdown of the clay matrix [12].

2.2.4 Permeation of water and contaminants

It has long been realized that transport paths in clay have the form of channels for migration of water, fluids, gas and ions and dissolved matter as generalized in Figure 8.

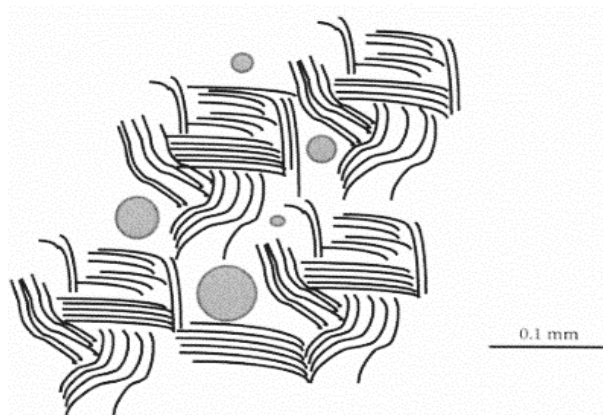


Figure 8: Microstructural model of hydrated montmorillonite and saponite clay with a bulk total density of 1,800-2,000 kg/m³ (Dry density 1,270-1,590kg/m³). For the lower density the bar is 0.1mm and for the higher density it is 0.0 mm [13,14].

A step to directly correlate the microstructural constitution of smectite buffer clay with lab investigations was recently made by Bouchelaghem and Pusch [15]. They modelled the hydraulic transmission of coupled “2D” TEM electron images by using the technique of “Homogenization of Periodic Media”, distinguishing between three levels: the microscopic level of clay particles, the mesoscopic level of clay aggregates, mineral grains and inter-aggregate porosity, and the macroscopic level of the sample subjected to hydraulic conductivity tests in the laboratory. Several cases were distinguished as soft and dense gels, open voids forming connected flow paths, or remaining occluded. For all three cases considered, starting from the local description of fluid flow, expressions of the effective hydraulic conductivity tensor were derived. The microstructure was obtained by image analysis of digitalized micrographs in order to obtain the contours of the different phases. These contours were then imported into a finite element-based software in order to solve the local problems. Numerical computations allowed the authors to investigate the contribution to macroscopic flow by the soft and dense gels in connected and non-connected configurations (cf. Figure 9).

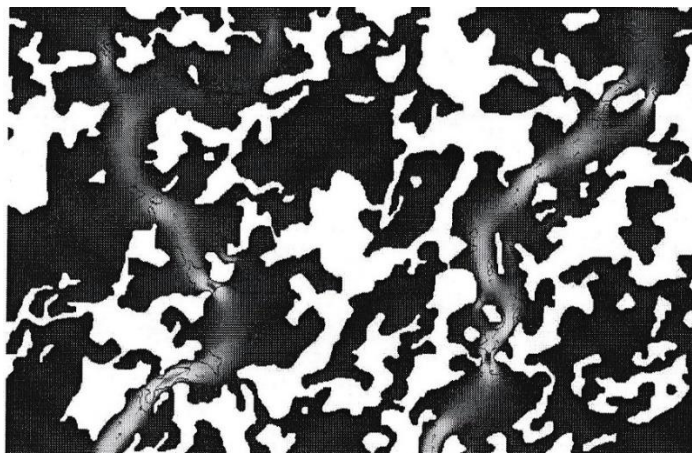


Figure 9: Identified connected macropores (grey) making up microstructural channels in smectite clay with $1,300 \text{ kg/m}^3$ (total) density. Magnification: $10 \text{ mm}=1 \text{ micrometer}$ [15].

These investigators modelled the hydraulic conductivity of compacted water-saturated smectite clay based on the real microstructure and the “*Homogenization of Periodic Media*” approach employed for deriving the permeability tensor. This has fully acknowledged the heterogeneous and multiscale microstructure of clay, as well as locally varying physical flow properties. In summary, the three levels of description considered, i.e. the microscopic level of clay particles etc, provided the basis of numerical calculation of the hydraulic conductivity. It agreed well with the experimentally determined conductivity and verified that such clays used for isolation of radioactive matter have several phases of soft and dense gels and open

voids forming connected flow paths or being occluded. For all three cases considered, starting from the local description of fluid flow, the expression of the effective hydraulic conductivity tensor was derived. The microstructure was derived from image analyses of digitalized electron transmission micrographs in order to obtain the contours of the different phases. The contours were then imported into a finite element-based software in order to solve the local problems. Numerical computations gave the contribution to macroscopic flow by the soft and dense gels in the connected and unconnected configurations.

The study strongly supports the applicability of an earlier model for through-flow of smectite-rich clay considered as a system of gelfilled channels of different size (cf. Figure 10) that led to the 3Dchan code worked out by Neretnieks and Moreno (2009) [16], and that has been successfully used for modelling flow through soft, medium-dense and dense smectite clays [13].

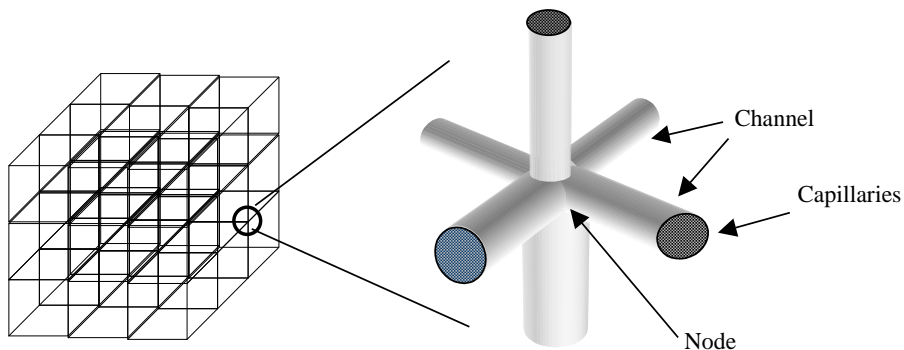


Figure 10: Schematic view of the 3D model concept with the channel network mapped as a cubic grid with channels intersecting at a node in the grid (After Neretnieks and Moreno).

The channels in the conceptual 3D model are characterized by their lengths, widths, apertures and transmissivities. The rest of the clay matrix is assumed to be porous but largely impermeable. Calculation of the bulk hydraulic conductivity is made by assuming that a number of channels (commonly taken as 6) intersect at each node of the orthogonal network. Each channel consists of a bundle of N capillaries with circular cross-section. The channels are assumed to have the length L and to contain N capillaries with diameter d , which are taken to be proportional to the channel width and match the total porosity of the clay. After complete maturation the voids, filled with homogeneous clay gels, are assumed to have a normal size distribution with the following void spectrum: 1-5 μm for 2,130 kg/m^3 bulk density at saturation (dry density 1790 kg/m^3), 1-20 μm for the bulk density 1,850 kg/m^3 at saturation (dry density 1,350 kg/m^3), and 1-50 μm for the bulk density 1,570 kg/m^3 at water saturation (dry density 904 kg/m^3). These sizes were determined from digitalized TEM 2D micrographs converted to represent 3D conditions [13].

2.3 Correlation of microstructural models and rheological behavior

2.3.1 Clay particle interaction

While most modellers make use of classical soil mechanical models that average stress conditions and base their reasonings on elasto/plastic theory we prefer to apply stochastic mechanics and do this by using what we call the Eyring/Feltham model, named after the creators [16]. It can be described as follows, starting by considering an element of soil or rock crystal matrix exposed to a shear stress that causes strain along an arbitrarily selected plane through the cubical element with “L” side-length (Figure 11). The passage of slip through the element displaces the part above the slip plane by an amount “b” resulting in shearing by b/L .

The model is taken to represent rate process theory and has the form of a time- and stress-dependent function controlled by the energy barrier spectrum on the molecular level. The evolution of strain depends on the energy required to overcome barriers representing the interparticle bond strength. This is a fundamental starting point for evolution of stress/strain relationships that lead to practically useful models for creep strain

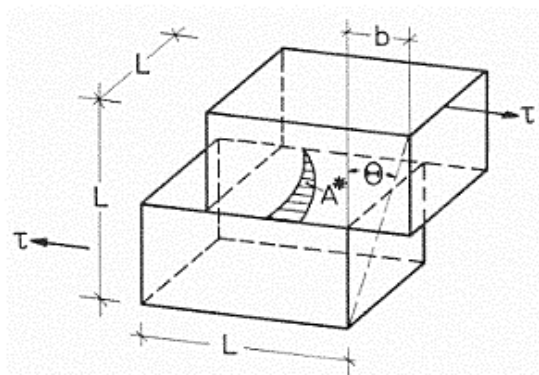


Figure 11: Element undergoing internal displacement caused by a slip unit jump generated by the local shear stress τ [16].

Following Pusch and Feltham [16,17] and assuming that interparticle slip has been activated at a certain point, meaning that an energy barrier has been overcome, a contribution to the overall shear strain has been made by the extension of the local slip-patch. Summarizing the various contributions in the element, a linear stress/creep-rate relation holds at very low stress levels, while at higher stresses the strain rate increases rapidly. Experience shows that stable conditions prevail for stresses lower than about 2/3 of the strength determined by using conventional methods – uniaxial compression, direct shearing, triaxial testing - according to which the strain rate tends to be successively lower, while for high stresses the creep tends to be proportional to time and ultimately leads to failure. For lower stresses than 1/3 of conventionally tested materials the strain rate commonly reaches a final definite value.

Equation 1 is an empirical expression that is generally referred to:

$$q = ap^b \quad (1)$$

where:

$a = q$ for $p = 1$ kPa

$b =$ inclination of curve in $\log p/\log q$ diagrams.

The experimental background is very limited but it is concluded from triaxial tests that a -values range between 2.8 and 5.5 depending on the porewater chemistry and type of adsorbed cation while b appears to have a constant value, 0.77.

Shearing takes place through the activation of barriers on the microstructural scale to slip. The barriers are represented by bonds of various kinds, from weak Van der Waals forces, via hydrogen bonds to strong primary valence bonds. They form a spectrum of the type shown in Figure 12, exhibiting spatial differences in barrier height.

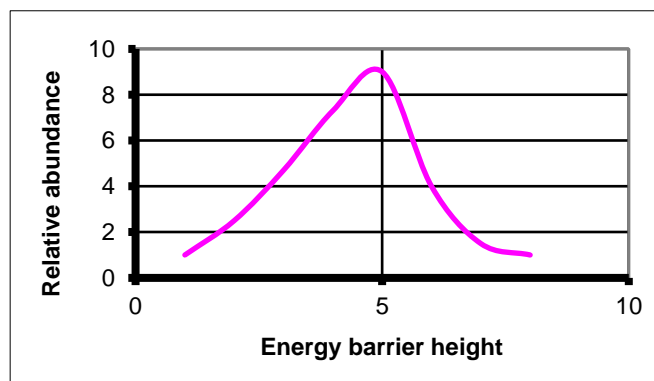


Figure 12: Schematic energy barrier spectrum.

Particle aggregates and individual particles of rock-forming minerals behave as strong units that remain intact for small strain but yield at large strain and contribute to the bulk strength by generating dilatancy. The energy spectrum is hence not a material constant but changes with strain and thereby with time. A fraction of the strain-induced microstructural changes are preserved but exfoliated montmorillonite stacks reorganize and cause self-healing by forming gels of different density depending on the available space and rate of strain. This means that local bond breakage is balanced by formation of numerous new bonds that make the altering microstructural network stay coherent for low and moderate bulk shear stresses, while higher shear stresses cause irreparable changes of the network leading to bulk failure at a certain critical strain.

The response of the structure to a macroscopic shear stress is that the overall deformation of the entire network of particles changes by disintegration, translation

and rotation of weaker aggregates while stronger ones are less affected. Breakdown of weak aggregates that are transformed to a laminated structure of flaky particles is illustrated by Figure 13.

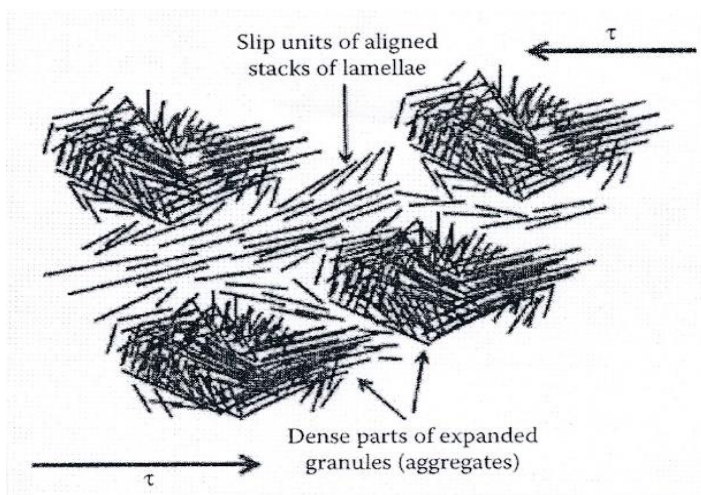


Figure 13: Formation of slip domains by shearing of weak particle aggregates in smectite clay.

For a clay element subjected to a constant deviator stress one can assume that the number of energy barriers of height u is $n(u,t)\delta u$ where δu is the energy interval between successive jumps of a unit, and t is the time. The change in activation energy in the course of evolution of strain means that the number of slip units is determined by the outflux from any u -level into the adjacent, higher energy interval and by a simultaneous influx into the interval from $u-\delta u$ [18].

Each element of clay contains a certain number of slip units in a given interval of the activation energy range and displacement of such a unit occurs as the shifting of a patch of atoms or molecules along a geometrical slip plane. The low energy barriers are triggered early and new slip units become enrolled at the lower end of the energy spectrum in Figure 12. This end represents a “generating barrier” while the high u -end is an “absorbing barrier”. A raised deviator stress affects the rate of shift of the energy spectrum only to higher u -values provided that the shearing process does not significantly reduce the number of slip units. This is the case if the bulk shear stress does not exceed a critical value, i.e. about 1/3 of the conventionally determined bulk strength and limits the bulk strain to be caused by the integrated very small slips along interparticle contacts. This can be termed “primary creep”.

For low bulk shear stresses, allowing for “uphill” rather than “downhill” jumps, one gets for the rate of change of $n(u,t)$ with time:

$$\frac{\delta n(u,t)}{\delta t} = \nu[-n(u+\delta u,t)\exp[-(u+\delta u)/kT] + n(u,t)\exp(-u/kT)] \quad (2)$$

where:

- δu =width of an energy spectrum interval
- ν =vibrational frequency (about $E11$ per second)
- t =time
- k =Boltzmann's constant
- T =absolute temperature

Using Equation (2) and introducing Feltham's transition probability parameter to describe the time-dependent energy shifts and that each transition of a slip unite between consecutive barriers gives the same contribution to the bulk strain one gets the bulk shear strain rate as in Equation (3) with $t < t_0$ as boundary condition:

$$d\gamma/dt = \beta(1-t/t_0) \tag{3}$$

where β is a stress-related material constant, and t_0 depends on the deviator stress, temperature and structural details of the slip process. The creep strain can be expressed as Equation 4, which implies that it starts off linearly with time and then dies out as exemplified by Figure 14.

$$\gamma = \alpha t - \beta t^2, (t < a/2\beta) \tag{4}$$

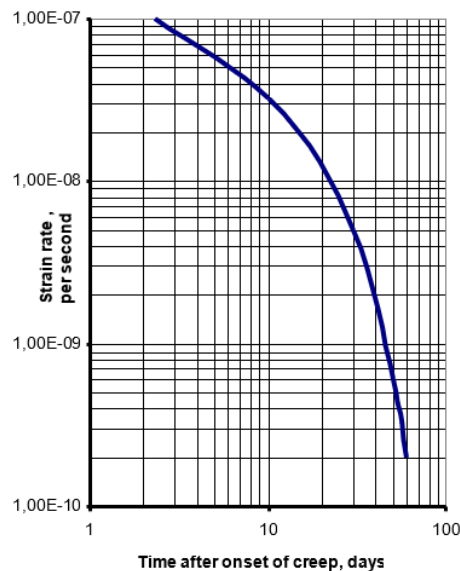


Figure 14: Creep strain of smectite-rich clay (MX-80) with a density at saturation with distilled water of 1,500kg/m³. Double shear box apparatus, average shear stress 6kPa.

For higher bulk stresses the strain on the microstructural level yields some irreversible changes associated with local breakdown and reorganization of structural units, like in Figure 13. Still, there is repair by inflow of new low-energy barriers parallel to the strain retardation caused by the successively increased number of slip units being stopped by meeting higher energy barriers. This type of creep can go on for ever without approaching failure. Following Feltham the process of simultaneous generation of new barriers and migration within the transient energy spectrum lead to the expression for the creep shear rate in Equation (5). Feltham demonstrated that for thermodynamically appropriately defined limits of the u -spectrum the strain rate appertaining to logarithmic creep takes this form [17,18]:

$$d\gamma/dt = BT\tau/(t+t_o) \quad (5)$$

where B is a function of the shear stress τ .

t_o is a constant of integration which leads to a creep relation closely representing the commonly observed logarithmic type implying that the creep strain is proportional to $\log(t+t_o)$.

The significance of t_o is understood by considering that in the course of applying a deviatoric stress the deviator rises from zero to its nominal, final value (Figure 15). A u -distribution exists at $t=0$, i.e., immediately after full load is reached, which may be regarded as equivalent to one which would have evolved in the material initially free from slips, had creep taken place for a time t_o before loading. Thus, t_o is characteristic of the structure of the prestrained material including the impact of cementing precipitations [18].

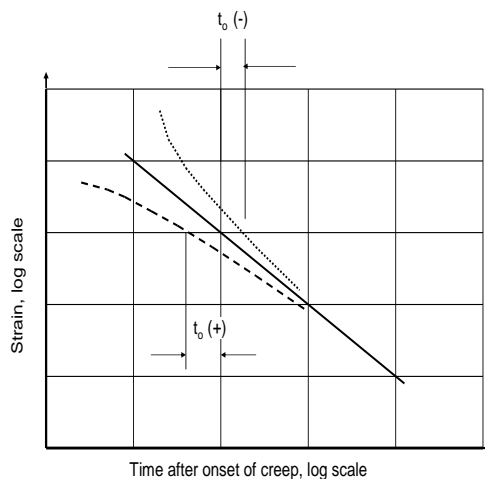


Figure 15: Generalization of creep curves of log time type showing the meaning of t_o .

There are two important implications of this model, firstly that the lower end of the energy spectrum mainly relates to breakage of weak bonds and establishment of new bonds where stress relaxation has taken place due to stress transfer from overloaded parts of the microstructural networks to stronger and more rigid parts. It also means that, for deviators below a critical level, the energy spectrum undergoes a “blue-shift”, meaning that the content of high energy barriers increases, as illustrated in Figure 16. The bulk shear strength hence increases with time, as does the bulk stiffness, which implies, in turn, that the system remains stable for very long periods of time exhibiting successive retardation of the creep, but that the clay becomes brittle and can collapse quickly if the bulk shear load is raised to a critically high level.

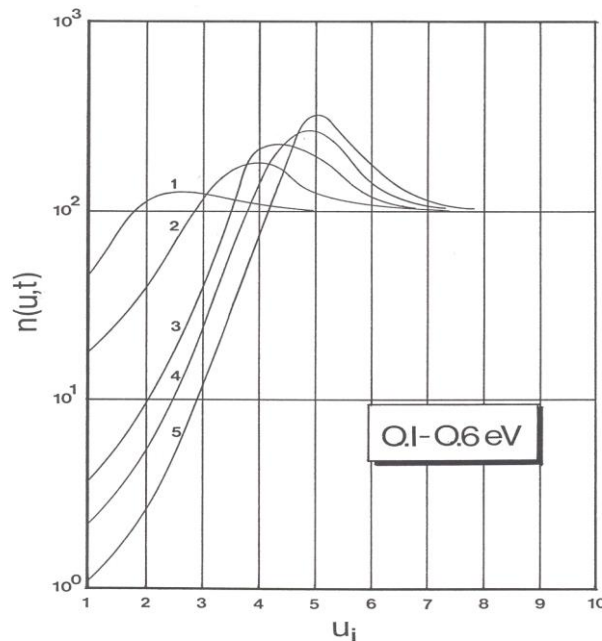


Figure 16: Example of activation energy spectrum for interparticle slip at different times after the onset of creep [18].

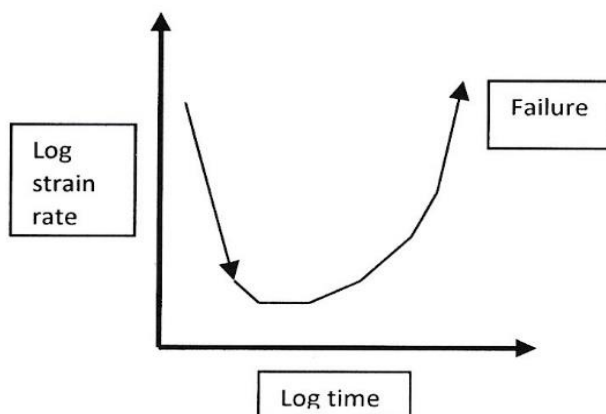


Figure 17: Evolution of creep for critically high shear stresses.

For intermediate bulk stresses actual creep tests of smectite-rich clay have given results exemplified in Figure 18.

Further increase in deviator stress leads to what is conventionally termed “secondary creep” in which the strain rate tends to be constant and causes strain that is almost proportional to time. Following the same reasoning as for the lower stress cases one can imagine that creep of critically high rate makes it impossible for microstructural self-repair: comprehensive slip changes the structure without allowing reorganization, which yields a critical strain rate which inevitably leads to failure (Figure 17). For smectite clay shear-induced formation of slip units, consisting of stacks of lamellae, is much more comprehensive than in illitic and kaolinite-rich clays. The successive increase in the number of slip units in fact implies an important self-sealing ability that causes attenuation of the creep rate of smectite-rich clay even for high shear stresses as indicated by the diagram in Figure 18. Figure 19 represents creep testing of smectitic clay indicating that smectite-rich clays under critically high shear stresses behave as Newton fluids and undergo “secondary creep” ending with failure in agreement with Figure 17.

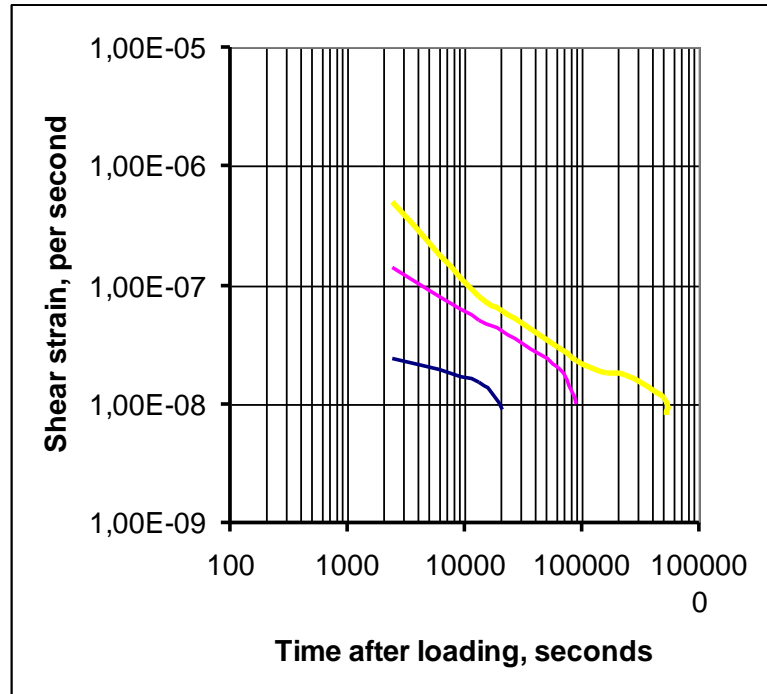


Figure 18: Creep strain of montmorillonite-rich clay (MX-80) for the average shear stresses 39, 23 and 11kPa (from top). Density at saturation with distilled water 1,940 kg/m³.

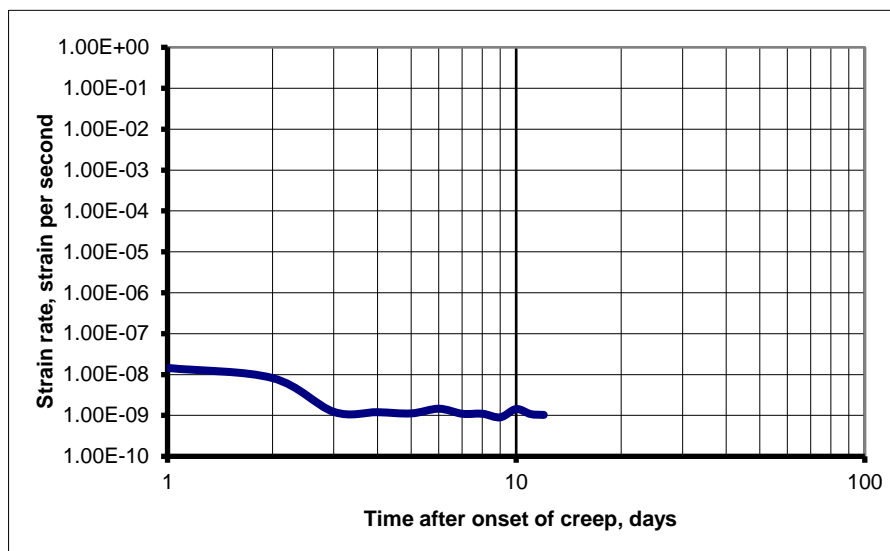


Figure 19: Creep of the same sample as in Figure 14 by increasing the shear stress to 23kPa. The creep rate attenuated but turned into a constant, relatively low strain rate without leading to failure in the two weeks long test performed at room temperature.

In summary, the following features of the creep model are assumed:

- Each element of clay contains a certain number of slip units in a given interval of the activation energy range and displacement of such a unit is taken to occur as the shifting of a patch of atoms or molecules along a geometrical slip plane (Figure 10). In the course of the creep the low energy barriers are triggered early and new slip units come into action at the lower energy end of the spectrum in Figure 16. This end represents a “generating barrier” while the high u -end is an “absorbing” barrier,
- A changed deviator stress affects the rate of shift of the energy spectrum only to higher u -values provided that the shearing process does not significantly reduce the number of slip units. This is the case if the bulk shear stress does not exceed a certain critical value, which is on the order of 1/3 to 2/3 of the conventionally determined bulk strength. The creep rate is initially linear with time, then drops and finally dies out. It implies that the microstructural constitution remains unchanged and that bulk strain corresponds to the integrated very small slips along interparticle contacts. In principle this can be termed “primary creep”
- For intermediate bulk shear stresses, allowing for “uphill” rather than “downhill” jumps on the energy spectrum, creep retards according to a log time function and reaches a finite specific value for a given period of time.

2.3.2 A typical creep case – the settlement of a 20 ton canister with spent fuel resting in dense “buffer” clay

The creep case considered here is illustrated by Figure 20, which shows a cross section of a repository at 400 m depth representing the concept of Swedish Nuclear Fuel and Waste Management Co (SKB). The integration of the soft clay mud in which the heavy supercontainer with canister and dense clay were submerged is assumed to have taken place, implying that the buffer clay (“bentonite”) has expanded and consolidated the mud. This process has been investigated in detail by Yang [19].

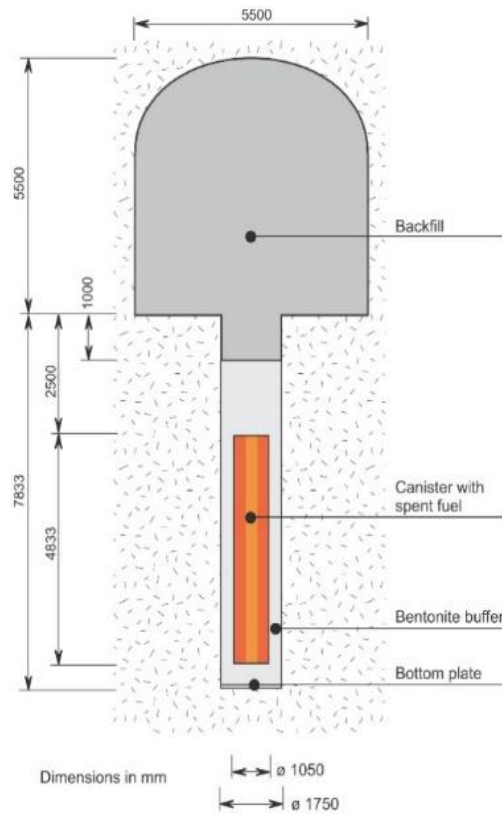


Figure 20: SKB's concept KBS-3V. The canister with spent fuel has a weight of about 25 tons [20].

The time-dependent settlement of the supercontainer was calculated by using Equation 6 and the boundary element (BEM) code BEASY worked out by Computational Mechanics Center (CMI, Southampton, England), which also made the calculations.

The diameter and height of the canister was 1.05m and 4.8m, respectively. It was assumed to rest on 0.5 m clay, be surrounded by 0.35m clay and covered by 1.5m clay, all confined in a bored hole with 7m depth in rigid rock. The E-modulus of the clay was taken as 300MPa and Poisson's ratio taken as 0.49. Room temperature was assumed.

The settlement rate was predicted by use of Equation 6, which is a generalized version of Equation 5 [21]:

$$ds/dt = \beta T D \ln t \quad (6)$$

$\beta = 3E-10 \text{ K}^{-1}, \text{ kPa}^{-1}$ = creep strain parameter evaluated from undrained triaxial tests of montmorillonite-rich clay with the dry density $1,590 \text{ kg/m}^3$ at room temperature.

$D = \sigma_1 - \sigma_2$ (average deviator stress), $\sigma_1 > \sigma_2 = \sigma_3$ principal stresses.

Table 2: Predicted settlement of full-scale canister at 20°C for $\beta=3E-10$ [$K^{-1}kPa^{-1}$] with and without slip along the contact between clay and rock and canister.

Time after onset of creep [sec]	Predicted settlement with slip along the contact between clay and rock [mm]	Recorded settlement without slip [mm]
E0	0.358	0.049
E1	0.426	0.058
E2	0.493	0.068
E3	0.560	0.077
E4	0.627	0.086
E5	0.695	0.095
E6	0.762	0.105

The calculated settlement assuming no friction/adhesion along the contact between clay and rock, will theoretically be between one third and half of a millimeter in 10-100 years. The rate of settlement then drops quickly and becomes $\frac{3}{4}$ of a millimeter after E6 seconds. In practice, the rate of settlement will be either slower because of the stiffening effect of precipitated silicious compounds, or faster because of compression as discussed later in the paper. Before examining the effect of such processes, we will describe a laboratory experiment of the same type.

2.3.3 Laboratory-scale experiment

The just described case of canister settlement was investigated by conducting a small-scale test that involved recording of the movement of a model canister embedded in the same type of dense montmorillonite-rich clay at constant temperature of 21.5-22.0°C (Figure 21). The clay was precompacted and trimmed to fit in the load cell with access to distilled water via a filter for 3 months, giving complete saturation at a density of 2,000kg/m³ (dry density 1,590kg/m³).

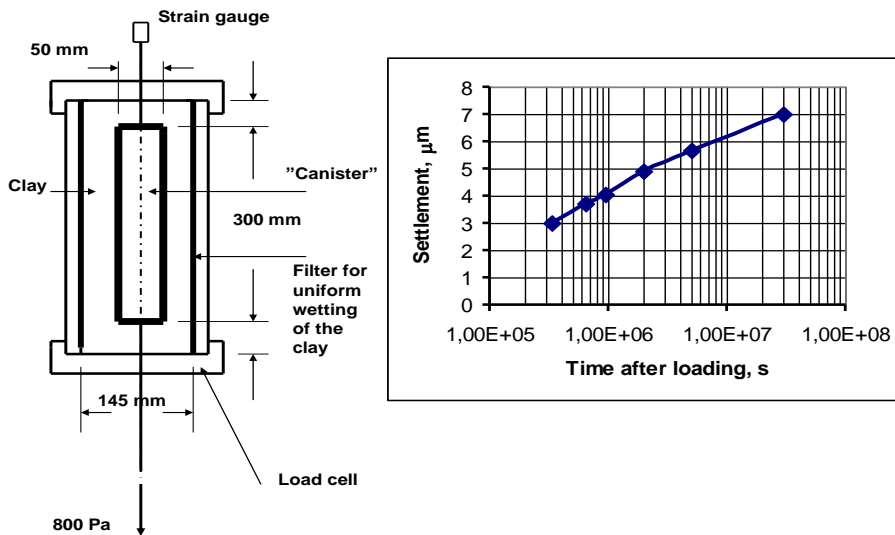


Figure 21: Experiment for determining the settlement of a model canister embedded in clay under drained conditions and carrying a dead-load of 800 N [21].

The 50mm diameter canister was loaded by 800N after 3 months of maturation of the clay with access to water from the filter-equipped container for homogenization. The contact pressure between the canister base and the clay, neglecting wall friction, was thence 400kPa. The settlement was recorded with an accuracy of E-4 μm . The load application caused settlement of visco-elastic type amounting to 2-3 μm in the first few hours. The total creep strain was about 6 μm after 2 months loading and about 7 μm after 3 months. It was approximately proportional to log time with a slightly dropping trend, approximately in agreement with Eq.5. The same type of settlement calculation as for the full-scale case with 20t canister in montmorillonite-rich clay with the same dry density, i.e. 1,590kg/m³ was made giving results that agreed well with the recorded ones as illustrated by Table 3. The predicted distribution of the vertical movements in the clay after E6 seconds is illustrated in Figure 22, showing that there would be upward movements in the clay up to about 25mm above the base of the canister, and that downward and lateral movements dominated below it.

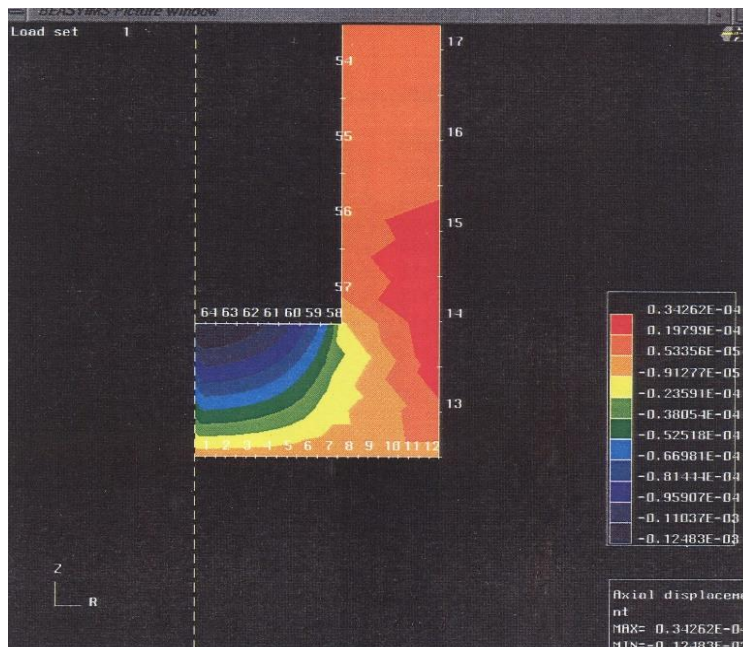


Figure 22: Calculated distribution of the vertical displacements in the clay 6E6 seconds after loading assuming slip along the clay/cell and clay canister contacts (minus represents upward movement, plus is upwards), [21].

Table 3: Predicted and actual settlement of the model canister at 20°C for $\beta=3E-10$ [K⁻¹ kPa⁻¹]

Time after loading [sec]	Predicted settlement [μm]	Recorded settlement [μm]
3E5 (0.01 y)	3.0	3.0
6E5 (0.02 y)	4.0	3.7
3E6 (0.10 y)	5.0	5.2
6E6 (0.20 y)	6.0	6.0

2.4 Creep behaviour of clay seals loaded by waste canisters in boreholes

Log-time creep behaviour of dense montmorillonite-rich clay for medium-high shear stresses has been frequently recorded in laboratory and bench-scaled investigations like the study by Al-Thaie et al, 2014 [22]. Their study also showed that even relatively low amounts of this mineral largely control the rheological behaviour of clays (Figure 23). According to the diagram in this figure the clay with 25% montmorillonite content gave slightly quicker retardation of the creep rate than the clay with 50% content of montmorillonite for any stress level, which can be ascribed to the higher content of strong barriers (non-clay minerals) of the first mentioned.

Secondary consolidation by long-term loading under drained conditions has the same character: the settlement of the canister approximately obeys the expression:

$$s=CH\ln(t_2-t_1) \quad (7)$$

where C =material coefficient, H =thickness of loaded clay layer, t_1 =time for start of settlement and t_2 =time for ending the period considered [10].

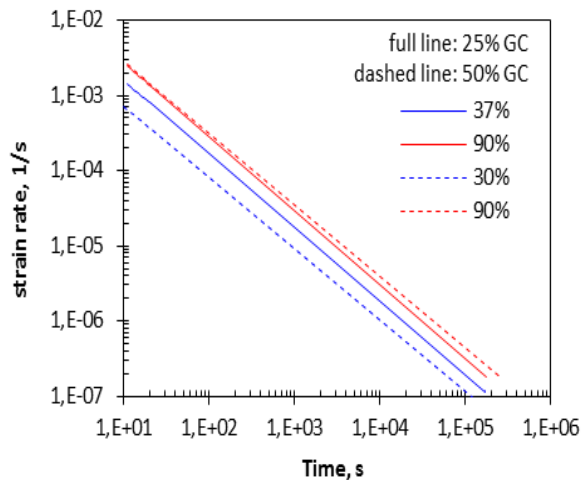


Figure 23: Strain rates for different shear stresses on equally dense clays with 25 and 50% montmorillonite content (GC). The percentages refer to the fraction of the conventionally determined shear strength of the respective clay [22]. All curves indicate, in principle, log time strain behaviour.

2.5 Physico/Chemical stability of montmorillonitic clays and its impact on creep behaviour

The physical and chemical stabilities of montmorillonite are classic matters in deep-boring technologies and are briefly commented in this paper.

2.5.1 Physical stability

A major problem to be considered is the risk of desiccation of the clay surrounding canisters in a KBS-3 repository located in very dry crystalline rock. Experience from full-scale field tests indicates that water saturation of the clay can require a hundred years or more and lead to fissuring that can be permanent when silica is precipitated according to the generally accepted mineral conversion process [1,22,23]:



The conversion to illite means that voids in montmorillonite increase in size and interconnectivity by which the average hydraulic conductivity increases by at least one order of magnitude and the swelling pressure is reduced by one- to two orders of magnitude depending on the type of adsorbed cation and degree of silicification.

For the deep-hole concept VDH, with dense montmorillonite clay forming multiple seals in the holes, water saturation and maturation is quick because of the high water (mud) pressure [14,24].

2.5.2 Chemical stability

Clay seals

Equation 7 has been used by a number of investigators for predicting the degradation rate of montmorillonite clay exposed to temperatures of up to several hundred centigrades for a million years using theoretical models based on the classic Arrhenius' equation [23,24,25,26]. The results indicate that for 100°C temperature, which is a recommended maximum by most regulators, the original montmorillonite content is expected to drop from 100% to 50% in E4 years and to 10% in E5 years. For 150°C during 1,000 years, which is the expected heat pulse for the lowest part of a VDH repository, the intact part of the montmorillonite would be 50%. As mentioned, silica cementation at this temperature would strongly reduce the expandability and self-sealing ability already after some decades. The expandability indicated in Figure 24 would be lost.

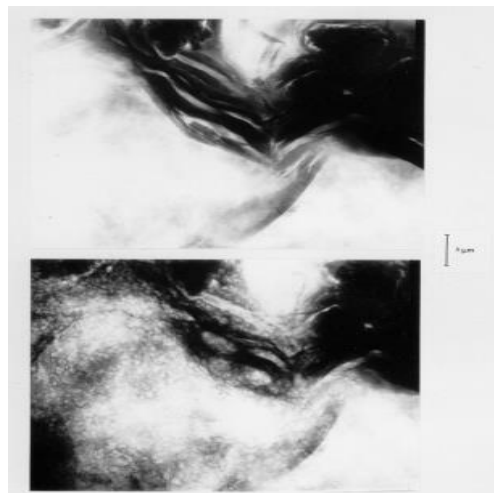


Figure 24: Montmorillonite depicted in CNRS' high-voltage transmission microscope. Upper: air-dry condition. Lower: the same specimen wetted and expanded by water saturation [27].

Concrete in deep holes

Concrete will be used for stabilization of deep deposition holes as indicated in Figure 1. Ordinary concrete with Portland cement as binder would be short-lived and degrade contacting clay seals, while use of low-pH cement and inorganic superplasticizers (talc) that do not give off organic colloids that can transport radionuclides, will do. The cement/clay reaction products contribute to the strength of the concrete [14,27].

3. Comments and conclusions

The following major conclusions from the study can be summarized as follows:

- The microstructure of smectite clay used for sealing off waste packages containing highly radioactive waste like spent fuel in repositories of mined type or consisting of deep boreholes controls the transport of water and ions as well as the rheological performance [28],
- Considerable microstructural changes are caused by the hydrothermal conditions, which are similar for the depth of mined repositories - 400-500 m - and for the upper parts of very deep holes - 1,000-2,000 m, but much more comprehensive at 2,000-4,000 m depth to which deep boreholes for disposal of such waste extend,
- Stress/strain performance of clays is significantly affected by contents of smectitic clays, especially of montmorillonite, even at contents as low as 25 %. The reason is the strong hydrophilic potential and role of porewater held in both intra- and extra-lamellar positions of such clays, which has an extreme particle surface area
- The intra- and interparticle bonds represent energy spectra ranging from very low levels to that of primary valence bonds, which explains the importance of shear stress: creep at constant water content is dominated by relative displacement of neighbouring particles that can be large without causing breakage of the particle network by successive self-repair via shifts of the interparticle bond energy spectrum ("blue-shift") as long as the bulk shear stress is moderate (Figure 25)



Figure 25: Microstructural constitution of montmorillonite-rich clay (MX-80) sample saturated with 10% CaCl₂ solution and hydrothermally treated at 95°C, placed in a shear box for shearing along the joint between the two box parts (brown line). Magnification 200x. On-falling LED light.

- The chemical stability of clay seals from 2,000-4,000 m depth in bored holes is lower than in shallow, mined, repositories because of the higher temperature, up to 150°C for a few centuries after placing HLW waste packages. The hydrothermal impact on clay microstructure causes aggregation, increased hydraulic conductivity and loss of ductility because of cementation by precipitation of silicious matter (Figure 26). The net isolating capacity of clay seals is, however, lower in shallow, mined repositories than in deep boreholes where there are no horizontal hydraulic gradients and where the groundwater has high density because of the high salt content making it stay at depth.



Figure 26: The clay sample in Figure 25 sheared after hydrothermal treatment at 95°C. The white object to the right is one of the shear box halves. The fracturing that took place in conjunction with dilatancy at about 20 % strain in the sheared direction (right to left) demonstrates brittle behaviour and lack of self-sealing ability of the clay. Magnification 200x. On-falling LED light.

References

- [1] Herbert, H. J., Kasbohm, J., Sprenger, H., Fernández, A.M. and Reichelt, C. (2008). Swelling pressures of MX-80 bentonite in solutions of different ionic strength. *Physics and Chemistry of the Earth*, vol. 33, 2008, (327-342).
- [2] Brady, P.V, Arnold, B.W., Freeze, G.A., Swift, P.N., Bauer, S.J., Kanney, J.L, Rechard, R.P. and Stein, J.S (2009). Deep borehole disposal of high-level radioactive waste, SANDIA REPORT 2009-4401, New Mexico/Livermore Calif. USA, 2009.
- [3] Pusch, R., Yong., R.N. and Nakano, M. (2018). *Geologic Disposal of High-Level Radioactive Waste*. CRC Press, Taylor and Francis Group.
- [4] Kehres, A. (1983). Isotherms de deshydratation des argiles. Energies d'hydratation Diagrammes de pores surfaces internes et externes. PhD thesis Université Paul Sabatier, Toulouse, France.
- [5] Yong, R.N., Nakano M. and Pusch, R. (2012). *Environmental Soil Properties and Behaviour*, CRC Press, ISBN 9781439845295.
- [6] Ichikawa, Y., Kavamura, K., Nakano, M., Kitayama, K. and Kawamura, H. (1998). Unified molecular dynamics/homogenization analysis. In: Proc. on International High-level Radioactive Waste Management Conference, Las Vegas, US.
- [7] Pusch, R., Muurinen, A., Lehtikoinen, J., Bors, J. and Eriksen, T. (1999). Microstructural and chemical parameters of bentonite as determinants of waste isolation efficiency. Final Report of EC Project Contract F14W-CT95-0012, European Commission, Brussels.
- [8] Pusch, R. (2008). *Geological Storage of Radioactive Waste*. Springer Verlag, Berlin-Heidelberg.
- [9] Murad, M.A., Guerreiro, J.N. and Loula, A.F.D. (2008). Micromechanical computational modelling of secondary consolidation and hereditary creep in soils. *Computer Methods in Applied Mechanics and Engineering*, Elsevier Publ. Co.
- [10] Terzaghi, K. (1942). *Theoretical Soil Mechanics*. Wiley, US.
- [11] Biot, M. (1955). Theory of elasticity and consolidation for a porous anisotropic soil. *J. Appl. Physics*, 26, 1955 (182-185).
- [12] Pusch, R. (1970). *Clay Microstructure*. Swedish National Council for Building Research, Document D:8, Stockholm, Sweden.
- [13] Pusch, R. and Yong, R.N. (2006). *Microstructure of Smectite Clays and Engineering Performance*. Taylor and Francis, NY, USA. ISBN10: 0-415-36863-4.
- [14] Pusch, R. (2015). *Bentonite Clay. Environmental Properties and Applications*. CRC Press, Taylor and Francis Group.
- [15] Bouchelaghem, F. and Pusch, R. (2017). Fluid flow and effective conductivity calculations on numerical images of bentonite microstructure. *Applied Clay Science*, 144, (9-18).

- [16] Pusch, R. (1979). Creep of soils. Ruhr-Universität Bochum, Schriftenreihe des Instituts fuer Grundbau, Wasserwesen und Verkehrswesen, Serie Grundbau Heft 5.
- [17] Feltham, P. (1968). A stochastic model of creep. *Phys. Stat. Solidi*, 30, (135-146).
- [18] Pusch, R. and Feltham, P. (1980). A stochastic model of creep of soils. *Geotechnique*, 30/4, (397-506).
- [19] Yang, T. (2017). Maturation of Clay Seals in Deep Boreholes for Disposal of Radioactive Waste, Ph. Thesis, Luleå Technical University, Luleå, Sweden.
- [20] Svemar, C. (2005). Cluster Repository Project (CROP). Final reãpr̃t of European Commission Contract FIR-CT-2000.20023, Brussels, Belgium.
- [21] Pusch, R. and Adey, R. (1999). Creep in buffer clay. SKB Technical Report TR-99-32. SKB, Stockholm, Sweden.
- [22] Al-Thaie, L., Pusch, R. and Knutsson, S. (2014). Hydraulic properties of smectite rich clay controlled by hydraulic gradients and filter types. *Applied Clay Science* 87, (73-80). <http://dx.doi.org/10.1016/j.clay.2013.11.027>.
- [23] Pytte, A.M. and Reynolds, R.C. (1989). The thermal transformation of smectite to illite. In: *Thermal History of Sedimentary Basins*. N.D. Naeser & T.H. McCulloh, eds. Springer Verlag (133-140).
- [24] Grindrod, P, and Takase, H. (1993). Reactive chemical transport within engineered barriers. In: *Proc. 4th Int. Conf. on the Chemistry and Migration Behaviour of Actinides and Fission Products in the Geosphere*, Charleston, SC USA, 12-17 Dec. Oldenburg Verlag 1994 (773-779).
- [25] Gueven, N. and Huang, W.L. (1990). Effects of Mg²⁺ and Fe³⁺ substitutions on the crystallization of discrete illite and illite/smectite mixed layers. Dept. Geosciences Texas Tech University, Exxon Production research Co, Houston, Texas, USA.
- [26] Kasbohm, J., Pusch, R., Nguyen, T.L. and Hoang, M.T. (2013). Lab scale performance of selected expandable clays under HLW repository near-field view. *Environmental Earth Sciences*, 69, (2569-2579).
- [27] Mohammed, M. H., Pusch, R., Al-Ansari, N., Knutsson, S., Emborg, M., Nilsson, M., and Pourbakhtiar, A. (2014). Talc-Based Concrete for Sealing Borehole Optimized by Using Particle Packing Theory. *J. of Civil Engineering and Architecture*, Apr. 2013, 7, 4, (440-455).
- [28] Warr, L.N., and Grathoff, G.H. (2010). Sealing of investigation boreholes: Mineralogical and geochemical borehole plug analyses. Technical Report, Swedish Nuclear Fuel and Waste Management Co., Ernst-Moritz-Arndt-Universität, Greifswald, Germany.